Effect of Silicon on the Metastable Eutectic Temperature of Fe–C–Si Alloys

Urko de la Torre, Jon Sertucha, Anna Regordosa, Jacques Lacaze

Effect of silicon on the metastable eutectic temperature of Fe-C-Si alloys

Urko de la TORRE[1], Jon SERTUCHA[1], Anna REGORDOSA[1], Jacques LACAZE[2]

1. Azterlan, Basque Research and Technology Alliance, Aliendalde Auzunea 6, E-48200 Durango (Bizkaia), Spain.
2. CIRIMAT, Université de Toulouse, CS 44362, 31030 Toulouse, France

Corresponding author J. Lacaze: Jacques.lacaze@ensiacet.fr

Abstract

An attempt has been made to establish experimentally the temperature along the metastable eutectic in the Fe-C-Si system, down to the invariant three phase eutectic involving austenite, cementite and an iron silico-carbide. This was carried out by standard thermal analysis using cups with a coating rich in tellurium that is known to impede graphite growth. It turned out that evaluating the metastable temperature is possible up to a silicon contents of 3.8 wt.%, beyond which the driving force for graphite growth becomes so high that the development of stable eutectic cells can no more be hindered. This is quite unfortunate for melt control on the foundry floor but triggers further study for understanding and describing graphite shape in cast irons.

Keywords: silicon cast iron, metastable eutectic, solidification, tellurium

Introduction

Most cast irons are essentially Fe-C-Si alloys with low levels of additives or impurities. Thermal analysis is used as part of quality control during the preparation of the cast irons prior to mold casting and various commercial systems are available. Thermal analysis can potentially be used to estimate both carbon and silicon content as described in a previous work for eutectic and slightly hypereutectic alloys (referring to the stable system) [1]. However, this possibility depends on the actual ability to avoid graphite precipitation and to complete solidification by the metastable eutectic whose temperature depends mainly on the silicon content. The previous study highlighted the limited knowledge of the metastable eutectic temperature in the Fe-C-Si system and the present study aimed to provide original and consistent data.

With the rather recent development of high-silicon cast irons, metastable silicocarbides (SCs) may appear along with cementite, either during solidification or by precipitation in the solid state. A comprehensive review of the literature on microstructures and corresponding phases was recently proposed by Kante and Leineweber [2]. In rapidly solidified alloys containing 3-11 wt.% Si, these authors studied the metastable two- and three-phase eutectic microstructures that could emerge. These observations were compared with the metastable liquidus of the Fe-C-Si system as predicted by the evaluation of Lacaze and Sundman [3] and the recent assessment of Miettinen et al [4]. The two calculated liquidus projections are superimposed in Figure 1-a, where good overall agreement is seen with differences starting at silicon content higher than 5 wt.%, due to the fact that the assumed SC formula was not the same, i.e., Fe_8Si_2C for the former evaluation and Fe_6SiC for the latter. Interestingly, the Miettinen et al. assessment reproduces a broader set of experimental information than the first assessment that was focused on the low silicon domain.

Figure 1-b is a projection of the stable and metastable eutectic lines on the temperature-silicon content axes. The metastable cementite/austenite eutectic is located a few degrees below the stable eutectic in the Fe-C binary system, and is easily reached at limited cooling rates due to the slow growth kinetics of the stable graphite/austenite eutectic. With the addition of silicon, the temperature difference increases to nearly 100°C at 5 wt.% Si, which is the upper limit of current silicon cast irons. Reaching the metastable eutectic is therefore increasingly difficult and can be achieved either by increasing the cooling rate or by preventing graphite nucleation and growth. Kante and Leineweber relied on the effect of cooling rate and indeed obtained

predominantly metastable microstructures. However, they reported that graphite precipitates were present in their castings in amounts that increased sharply with silicon content. Thus, the real possibility of changing completely from stable to metastable solidification by increasing the cooling rate has intrinsic limitations.

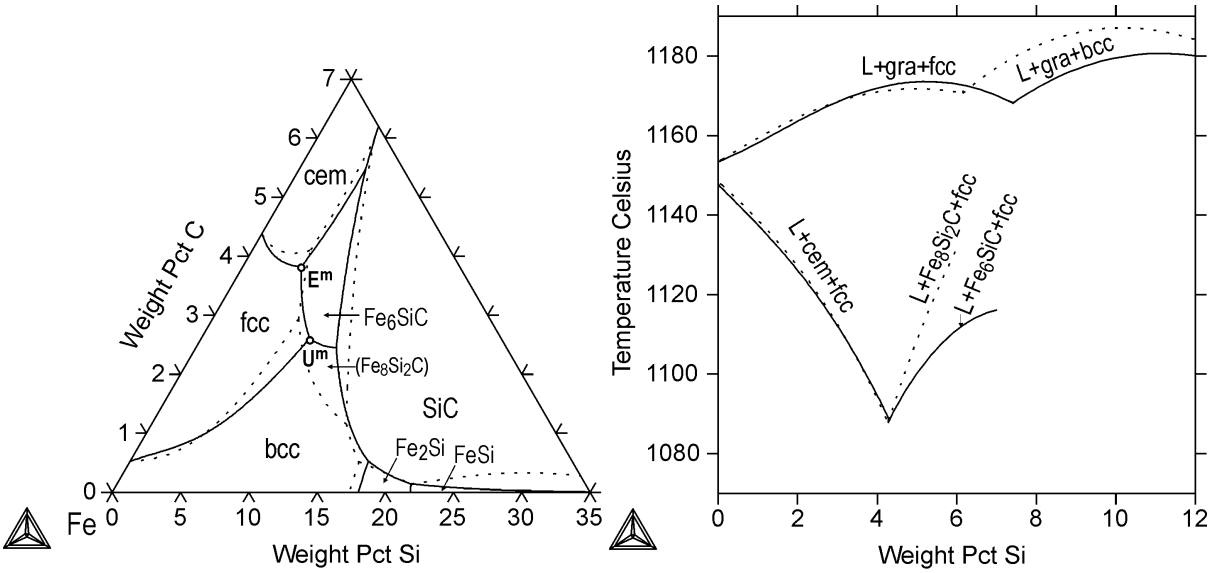

(a) (b)

Figure 1. (a) liquidus projection of the metastable Fe-C-Si system and (b) Evolution of the stable and metastable eutectic temperatures with silicon content. Dashed and solid lines are according to Lacaze and Sundman [3] and Miettinen et al. [4], respectively. These figures have been kindly provided by J. Miettinen and V. Ville-Valtteri (bcc: ferrite; fcc: austenite; cem: cementite; gra: graphite; L: liquid)

For the present study, the alloys were cast in commercial thermal analysis cups containing tellurium which is known to inhibit graphite growth [5, 6]. A series of experiments was performed where a base melt with 1 wt.% Si was prepared and gradually enriched to 5.64 wt.% Si. Thermal analysis showed consistent results for silicon contents up to, but not beyond, 3.8 wt.%. Metallographic analysis was performed for high silicon samples to determine their solidification microstructure and to clarify the limitations of this technique.

Experimental details

The objective during the trial was to maintain a melt composition close to the stable eutectic while the silicon content was to be increased by steps of 0.2 wt.% from 1 wt.% up to 6 wt.%. For this, a melt was prepared in a 100 kg capacity medium frequency furnace (250 Hz, 100

kW) with a metallic charge made up of 30 kg of low alloyed ferritic ductile iron returns and 40 kg of low alloyed steel. The carbon and silicon contents were adjusted using pure graphite and FeSi75 master alloy, respectively, and the first melt contained 3.88 wt.% carbon and 1.04 wt.% silicon (see table 1). Further increase in silicon was achieved by adding an appropriate amount of FeSi75 alloy according to the metallic mass present in the furnace. During the test, the decarburization of the melt by reaction with oxygen due to holding in the furnace and the relative decrease in carbon content due to the addition of FeSi75 were expected to ensure a steady decrease in carbon content so as to more or less follow the stable eutectic line (see Figure 10-a).

The furnace was kept at low induction power to maintain a near-constant temperature of 1450ºC, which ensured reproducible casting conditions throughout the test. For each composition, a medal sample for subsequent chemical analysis was poured, as well as five standard cups for thermal analysis (TA) in which a Te-rich patch was glued. The two types of cups available from Heraeus Electro-Nite are shown in Figure 2, which have the same external shape but with a square (SQ) or round (RD) cavity whose dimensions are listed in the legend to Figure 2. Repeat samples poured into the same type of cup were used to assess repeatability. The gray spot at the bottom of the cavity is the Te-rich coating. During the course of the test, the appearance of recalescence at the 4.49 wt.% silicon content (casting 18) led to the replacement of some of the single Te-coated cups with double Te-coated cups. The SQ double-Te cups were supplied by Heraeus Electro-Nite while the RD double-Te cups were prepared by hand gluing a second Te patch onto the existing one. In the following sections, the samples will be referenced by two numbers separated by a dot, the first number being the melt number (1 to 22) and the second indicating the type of cup (2 and 3 being RD, and 4, 5, 6 being SQ). For a single Te coating, independent measurements have shown that the maximum amount of tellurium transferred to the melt is on the order of 500 ppm, but that the amount remaining in the melt decreases rapidly if the tellurium is not tight in compound form [7].

All medal samples were analyzed using a combustion technique (LECO CS300) to determine carbon and sulfur content, while spark spectrometry (SPECTROLAB) was used to determine the content of all other elements. In the case of silicon, however, spark spectrometry was replaced by a gravimetric method for contents above 3 wt.%. The compositions of the alloys prepared in this work are listed in Table 1 where it can be seen that a maximum silicon

content of 5.64 wt.% could be achieved. It is also noted that the only element other than Fe, C and Si, which showed a non-negligible content is Mn, although at a low value of 0.13 wt.%.

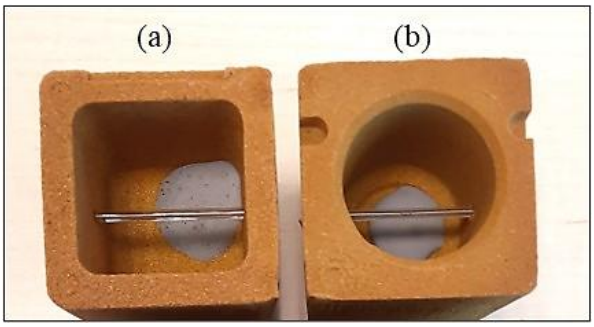

Figure 2. Upward view of the two different TA cups used in the present work: SQ cup (a) and RD cup (b). The grey patch at the bottom of the cavities is the Te-rich coating. The horizontal quartz tube protects the thermocouple whose junction is located in the middle of the cup. SQ cup cavities have a conical parallelepiped shape with a bottom base 35x35 mm, a upper base 37x37 mm and a height of 40 mm. The RD cups define a cylindrical volume with 34 mm in diameter and 40 mm in height.

The cooling curves were recorded using a data logger and a few examples are shown in Figure 3. All curves showed two thermal arrests, a short one that corresponds to austenite formation (denoted T_{LA} in the following) and then a longer one that relates to the eutectic reaction. Metastable solidification recorded by thermal analysis is generally associated with a flat horizontal plateau [8, 9], as reflected in the curve of sample 17 in Figure 3. This is due to the fact that the solidification front progresses in a columnar shape from the outer surface to the central part of the sections, with latent heat being removed by the solid rim [7]. In some rare cases, such as sample 6 in Figure 3, the plateau is almost flat but with slightly decreasing temperature. In this case, the temperature considered as characteristic of the plateau is that for which the time derivative of the curve is maximum. For high silicon contents, the cooling records showed a recalescence as illustrated by the curve of sample 22 in figure 3. In this case, the eutectic transformation can be characterized by the minimum temperature, $T_{e,min}$, before recalescence and the maximum temperature, $T_{e,max}$, reached during recalescence.

The temperature considered as characteristic of the eutectic transformation is that of the flat plateau in case of no recalescence or $T_{e,min}$ in case of recalescence. This choice is highlighted by the short dashed horizontal lines in Figure 3, and these temperatures will all be referred to as $T_{e,min}$ in the following for ease of reading.

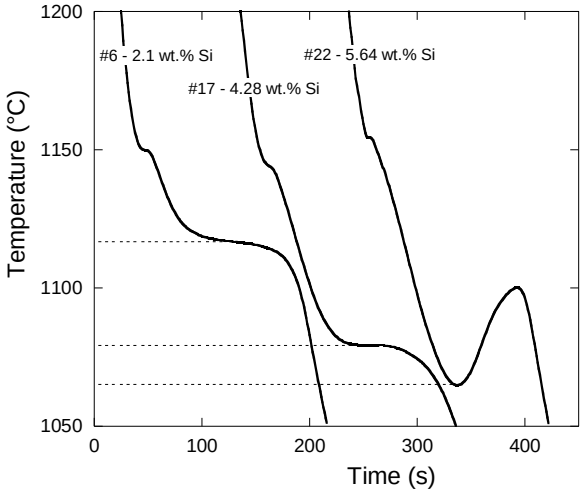

Figure 3. Records made with alloys 6, 17 and 22, cylindrical cup. The short dashed horizontal lines depict the eutectic characteristic temperature for each curve.

Results

The curves were all analyzed to evaluate, T_{LA}, $T_{e,min}$ and recalescence Rec ($Rec=T_{e,max}-T_{e,min}$), and all values are listed in Table AI in the appendix A. The values of $T_{e,min}$ and recalescence have been plotted in Figure 4-a as a function of silicon content. For silicon content up to 4.21 wt.% (alloy 16), the data from all five cups show high consistency with $T_{e,min}$ dispersion limited to less than ±1.5°C and no or very low recalescence. The transition is best seen in Figure 4-b which is an enlargement of Figure 4-a for the high silicon content range. At 4.28 wt.% Si and above, the $T_{e,min}$ values evaluated with the 5 curves for each alloy become more dispersed and significant recalescence appeared for some of the records at 4.49 wt.% Si (alloy 18) and above. Since this behavior is generally associated with the growth of stable eutectic cells, it was decided to also use double-Te cups for subsequent casts. In any case, almost all records showed significant recalescence for silicon contents above 5 wt.%, with some values reaching 30-70°C.

Thus, a clear transition was observed with increasing silicon content, with first a dispersion of $T_{e,min}$ values from 4.28 wt.% Si (alloy 17), and then an increase in recalescence values from 4.49 wt.% Si (alloy 18). The question therefore arose as to whether the appearance of SC could explain this behavior, especially in view of the very high recalescence values that were reached and which would normally indicate that eutectic solidification took place in the stable system. In the Appendix B, it is shown that SC could indeed be detected but at low levels in agreement with the results of Kante and Leineweber [2] for silicon contents such as those of

the present work. Such small amounts could hardly support an alternative SC-related solidification pathway, and it was therefore decided to study the microstructure of alloys 16 to 22 quite systematically.

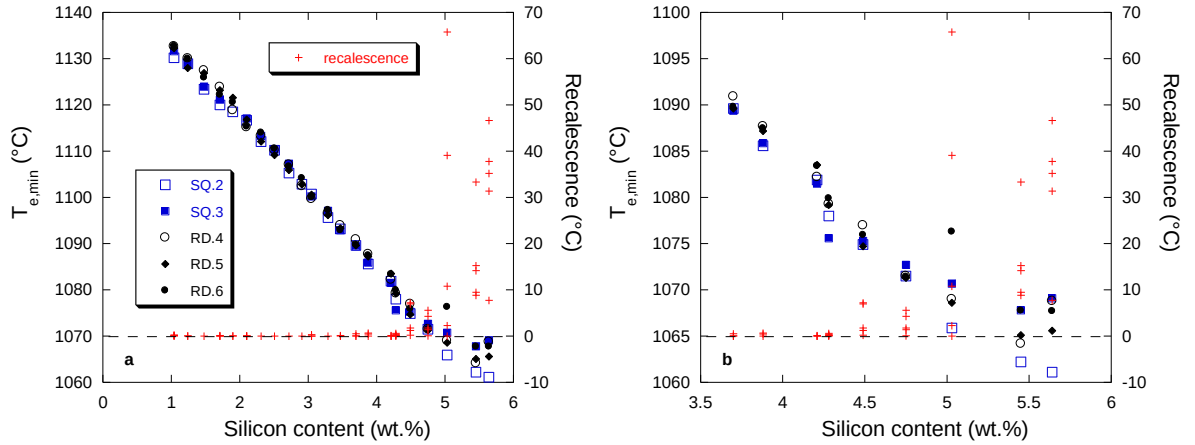

Figure 4. $T_{e,min}$ and recalescence values as function of the silicon content for the whole series of records (a) and enlarged view limited to high silicon contents (b). The horizontal dashed line corresponds to zero recalescence. Symbols in (b) are the same as in (a).

A first step in understanding the effect of increasing silicon content was to observe the microstructure of alloy 16 with 4.21 wt.% Si. As shown in Figure 4-b, all cups cast with this alloy showed very little recalescence and their microstructure should be similar. Figure 5 presents the microstructure of sample 16.5 chosen as an example. Unexpectedly, Figure 5-a before etching evidences quite a large amount of graphite, indicating that many stable eutectic cells have developed, while the many carbide plates left white after etching in Figure 5-b demonstrate that much of the eutectic solidification has, however, taken place in the metastable system.

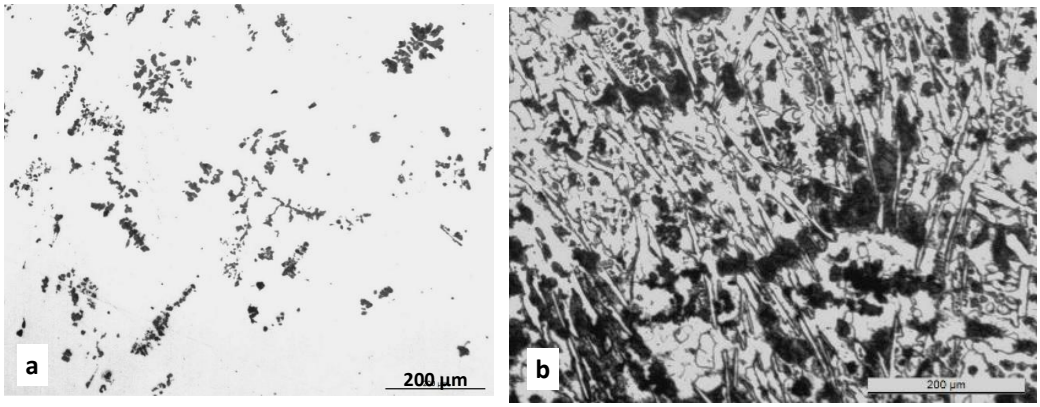

Figure 5. Micrographs of sample 16.5 before (a) and after (b) Nital etching.

Considering now the cooling curves that displayed recalescence, Figure 6 shows the five records for alloy 18 (Fig. 6-a) and for the last alloy 22 (Fig. 6-b). For alloy 18, the recalescence is still quite low for the three records with RD cups while it is already significant for the two records with SQ cups. The micrographs of sample SQ 18.3 are presented in Figure 7, before and after Nital etching. The first shows significant graphite precipitation between a dendritic structure, while some plate-like carbides are easily observed after etching. The microstructure of the other SQ sample 18.2 which showed a similar recalescence was identical. It can be inferred that all three RD samples of alloy 18 also had graphite, as was the case with sample 16.5 in Figure 5-a.

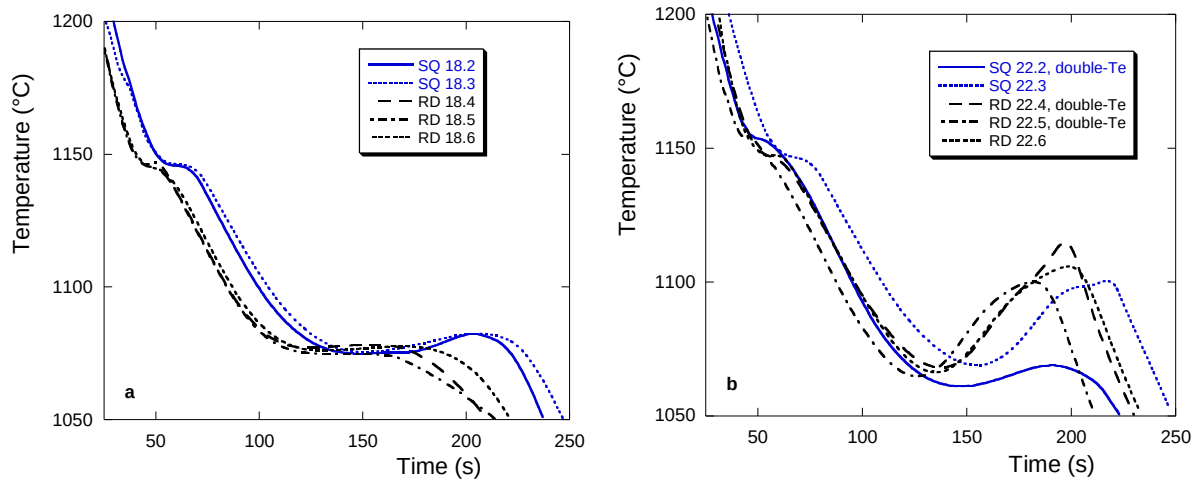

Figure 6. Cooling curves corresponding to all the samples from melts 18 (a) and 22 (b). All cups were single-Te for test 18 while some were double-Te for test 22 as indicated in the caption of (b).

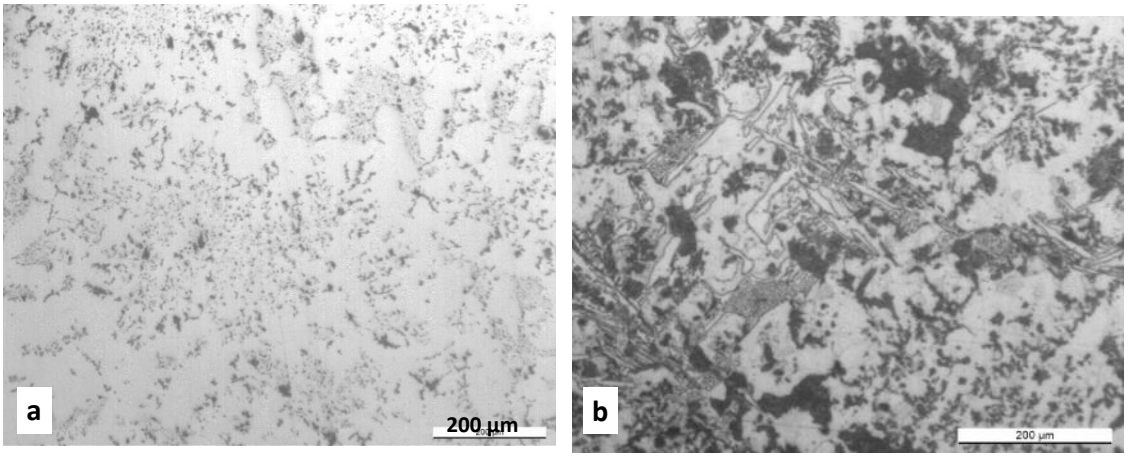

Figure 7. Micrographs of sample 18.3 before (a) and after Nital etching (b).

The cooling curves of alloy 22 at 5.64 wt.% Si all showed significant recalescence that was minimum for double Te-coated SQ sample 22.2 whose microstructure is illustrated in Figure 8. From the micrograph before etching (figure 8-a), it could be concluded that the microstructure is essentially graphitic but some carbide plates were observed after Nital etching (figure 8-b). In contrast, the simple Te-coated SQ sample 22.3 did not present any carbide. From these two samples, it would be concluded that the use of double-Te coating was effective in decreasing graphite precipitation and thus recalescence in SQ cups. However, Figure 6-b shows that this did not prevent graphite growth in RD cups as they all three showed huge amount of recalescence.

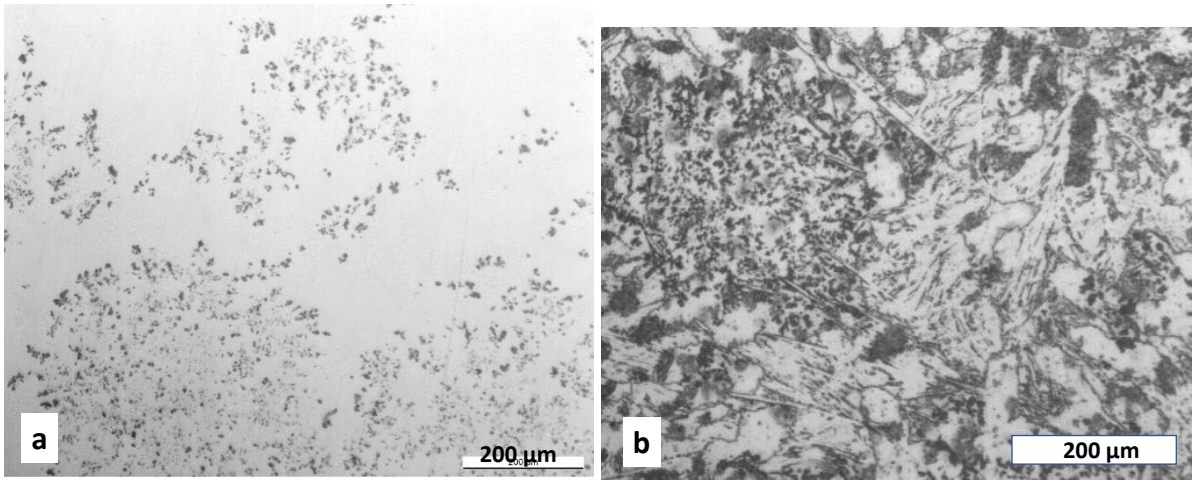

Figure 8. Micrographs of SQ sample 22.2 before (a) and after (b) Nital etching.

Discussion

From the metallographic observations presented above, it is concluded that recalescence of high-silicon alloys is related to precipitation of graphite/austenite eutectic cells and not related to the formation of a SC. In a previous study on thermal analysis of cast irons with silicon content of less than 3.8 wt.%, it was proposed that a record would still be valid for evaluating the metastable eutectic temperature if recalescence were lower than 5°C [1]. For such low recalescence values, it was understood that only a few cells of stable eutectic have nucleated and grown in the liquid ahead of the metastable eutectic front. Their number was however not large enough for the associated latent heat release to affect the metastable eutectic temperature indicated by the eutectic plateau. The question then arises whether this criterion can be applied to the higher silicon contents studied in this work.

Figure 4-b showed that at high silicon contents, samples SQ 2 and RD 5 had the lowest $T_{e,min}$ temperatures for each alloy. These two sets of results were therefore selected for further discussion and Figure 9-a shows the effect of silicon content on $T_{e,min}$ as in Figure 4 but here considering only these two cups and records meeting the above criterion. A regular and close evolution of the values is observed for these two cups, even for high silicon contents. In this figure are also shown the data evaluated in a previous work which was limited to 3.8 wt.% Si [1]. For silicon contents below 3.5 wt.%, the previous and current data sets agree well with each other. However, nearer to 4 wt.%, the previous data suggest a steeper slope with increase in the Si content than the current work.

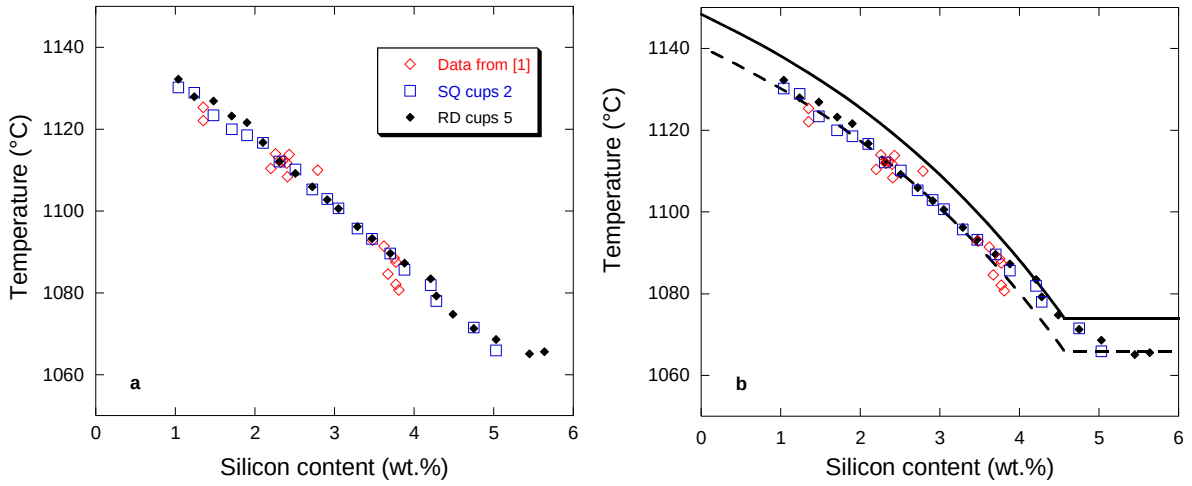

Figure 9. (a) Plot of experimental $T_{e,min}$ values assessed in a previous work [1] and measured on the SQ 2 and RD 5 cups during the present work, selecting values with recalescence lower than 5°C. (b) Same plot with superimposed the metastable eutectic temperature calculated with the TCFE-8 database (solid curve), with the horizontal part corresponding to an invariant three-phase eutectic (see text). The dashed curve was obtained by shifting downwards by 8°C the solid curve to account for eutectic growth undercooling in thermal analysis.

The present results would thus be at change with respect to the predicted evolution (see Figure 1-b) while older results are in line with them [1]. This discrepancy is illustrated with figure 9-b where the decreasing solid line represents the metastable austenite-cementite eutectic temperature in the Fe-C-Si system as calculated with the TCFE8 databank [10] that ends at the three-phase austenite-cementite-SC eutectic at 1074.4°C and 4.5 wt.% Si. The occurrence of this invariant eutectic is emphasized with the horizontal solid line in the graph. Note that this temperature for the three-phase ternary eutectic is slightly lower than the one appearing in

figure 1-b, certainly because of slight modifications in the TCFE database with respect to the original assessment [3]. Like any eutectic, the growth of the austenite-cementite eutectic takes place with some undercooling. An average value of this undercooling was estimated at 8°C by shifting the equilibrium solid curve downwards as represented by the dashed curve in Figure 9-b. Such a value agrees with estimate of the effect of cooling rate experimentally established by Oldfield and Humphreys [11] that has been previously discussed [1]. The horizontal line representing the invariant ternary eutectic has been shifted by the same amount. It is seen that the present and past experimental $T_{e,min}$ values closely follow the dashed line up to the critical silicon value of 3.8 wt.%, but then diverge at higher silicon contents, while the few results from the previous study at 3.6-3.8 wt.% Si do nicely fit with it.

The solid curve in Figure 9-b could be fitted by a second order polynomial of the silicon content, that was then shifted downwards by 8°C as in the previous work [1]. The temperature along the dashed line in figure 9-b that corresponds to the metastable eutectic as evaluated with a thermal analysis cup is thus given as:

$$T_{EW}^{cup} = 1139.6 - 7.16 \cdot w_{Si} - 1.94 \cdot w_{Si}^2 \qquad (1)$$

It is interesting to note that the second-order equation proposed by Glover et al. [12] based on unpublished experimental data, for silicon contents up to 3 wt.%, predicts values very close to those given by equation 1. The small difference between the two equations is positive at 0.9°C for 1 wt.% silicon and negative at 1.3°C for 3 wt.% silicon.

Some ambiguity might have remained about the value of using the calculated metastable eutectic temperature as a reference for silicon contents above 3.8 wt.% if the microstructures of the samples had shown small amounts of graphite. On the contrary, the presence of significant amounts of this phase suggests that the offset of the measured temperatures from the dashed line is a strong indication that the records were in fact invalid. This is particularly troublesome for its two consequences:

- The criterion that was previously defined to validate a cooling curve to estimate the metastable eutectic temperature, i.e. that the recalescence must be limited to less than 5°C, is not valid for silicon contents higher than a critical value which certainly depends on the cooling rate and which is here estimated at 3.8 wt.%.

- Standard thermal analysis cups, even with the addition of tellurium, have no potential for the evaluation of the metastable eutectic temperature for a silicon content above this critical value.

On a more basic point of view, it is interesting to realize that tellurium is effective for favoring metastable solidification at low and not at high silicon content. This may be rationalized by evaluating the driving force for graphite precipitation as function of the silicon content. In figure 10-a is plotted the evolution of the composition of the stable and metastable eutectics in the composition plane (w_C, w_{Si}) and the symbols represent the experimental alloys of the current work. It is seen that these alloys are close to the stable eutectic as expected, and that the carbon content in the liquid of the metastable eutectic diverges significantly as the silicon content increases.

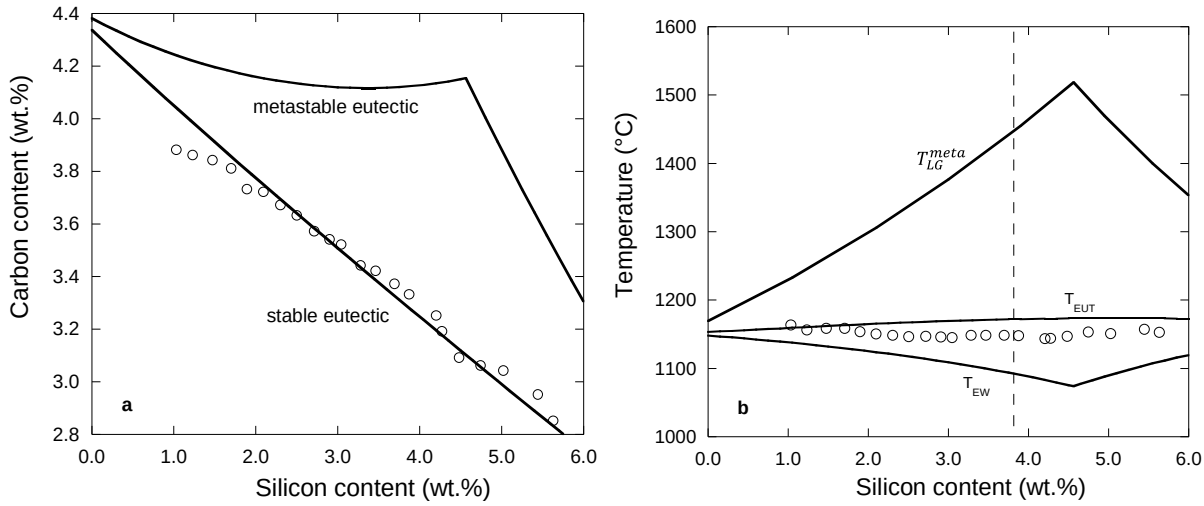

Figure 10. (a) plot of the composition of the stable and metastable eutectic lines calculated with TCFE8 with superimposed the composition of the investigated alloys (open circles). (b) Calculated temperatures T_{EUT}, T_{EW} and T_{LG}^{meta} (solid lines) and experimental T_{LA} temperatures for cup 5 (open circles). The dashed vertical line is positioned at 3.8 wt.% Si.

Figure 10-b shows with solid curves the evolution with the silicon content of the calculated temperatures of the stable (T_{EUT}) and metastable (T_{EW}) eutectics as well as that of the graphite liquidus for the carbon content corresponding to the metastable eutectic, noted T_{LG}^{meta}. On this graph have also been reported the T_{LA} temperatures measured during this work on cup 5. As expected, the T_{LA} temperatures are found to be very close to the temperature of the stable eutectic, which has the interesting effect of ruling out the possibility that graphite nucleated as

the primary phase. Instead, graphite must have appeared during austenite growth as the carbon content in the liquid gradually enriched toward the metastable eutectic.

A value by excess of the driving force for graphite precipitation is given by the temperature difference between the graphite liquidus temperature when the metastable eutectic is reached and the metastable eutectic temperature, $\Delta T = T_{LG}^{meta} - T_{EW}$. Figure 10-b shows that this quantity does strongly increase with the silicon content. As a matter of fact, it is known that fully white structures can hardly be obtained at silicon content higher than 2 wt.% for usual casting conditions. The corresponding ΔT value is 170°C, while further increase of the silicon content to 3.8 wt.% leads to ΔT=350°C that can be considered as the limit beyond which impediment of graphite growth is no more effective enough for the cooling conditions experienced in thermal analysis.

It can be claimed that tellurium efficiently inhibits the growth of graphite up to 3% silicon, then restricts this growth less and less when silicon is increased beyond that value because the driving force ΔT increases. While the cup is solidifying, cells of stable eutectic nucleate and grow just ahead of the metastable eutectic front moving from the outer surface to the center of the cup. At 3 wt.% Si, growth of the stable eutectic is limited because ΔT remains relatively low and this does not affect the thermal record. On the contrary, at silicon content larger than 4.5 wt.% ΔT has increased significantly and the growth of the cells of stable eutectic leads to recalescence and hence to an increase of $T_{e,min}$ above the metastable eutectic temperature. In the current work, the transition between these two cases occurred at 4.21 wt.% silicon (alloy 16) with eutectic plateaus that were flat but at a temperature that has been shifted upwards by the latent heat release ahead of the metastable eutectic front.

Conclusion

The description of the effect of silicon on the metastable eutectic by a second-order polynomial as previously suggested appears to be supported by the present work, even though valid experimental temperatures could not be measured for alloys with silicon content above 3.8 wt.%. This can therefore be considered as the upper limit for estimating silicon content based on standard thermal analysis. From a more fundamental perspective, the fact that tellurium can inhibit graphite growth up to and not beyond a critical undercooling below the

graphite liquidus is of fundamental interest to better understand the shape and growth of graphite in cast irons.

Acknowledgments

We warmly thank Alexandre Freulon, Cédric Charvillat and Yannick Thébaut from CIRIMAT for their help in the metallographic preparation, X-ray recordings and SEM observations.

Statement of interest

The authors declare that they have no conflict of interest

References

[1] A. Regordosa, J. Lacaze, J. Sertucha, M.J. Castro-Roman, U. de la Torre and O. Dezellus: Int. J. Metalcast. DOI: 10.1007/s40962-022-00799-5

[2] S. Kante and A. Leineweber: J. Alloys Compds., 2020, vol. 815, p 152468.

[3] J. Lacaze and B. Sundman: Metall. Trans. A, 1991, vol. 22, pp. 2211-2223.

[4] J. Miettinen, V. Ville-Valtteri and T. Fabritius: Thermodynamic Description of the Fe-Al-Mn-Si-C System for Modelling Solidification of Steels, Oulun yliopisto, Oulu, 2019. http://jultika.oulu.fi/Record/isbn978-952-62-2251-6

[5] H. Nieswaag and A.J. Zuithoff: Solidification structures and graphite patterns in tellurium-treated grey cast iron, 34th International Foundry Congress, 1967, paper 19

[6] N. Tsutsumi, M. Imamura and M. Nakada: The influence of tellurium on the graphite formation of cast iron during solidification, report 28 of the Castings Research Laboratory, Waseda university, 1977

[7] U. de la Torre, A. Regordosa, J. Lacaze, E. Aguado and J. Sertucha: Materialia, 2023, vol. 27, p. 101665, https://doi.org/10.1016/j.mtla.2022.101665.

[8] W. Menk, M.O. Speidel and R. Döpp: Giessereiforschung, 1992, vol. 44, pp. 66-79.

[9] D.M. Stefanescu: Inter. J. Metalcast., 2015, vol. 9, pp. 7-22.

[10] Thermocalc softwares and databases, https://thermocalc.com/products/

[11] W. Oldfield and J.G. Humphreys: BCIRA J., 1962, vol. 10, pp. 315-324.

[12] D. Glover, C.E. Bates and R. Monroe: AFS Trans., 1982, vol. 90, pp. 745-757.

Table 1. Chemical composition of the cast alloys (wt.%).

** indicates when double-coated cups were used

Trial number	C	Si	Mn	P	S	Cr	Ni	Cu	Ti	Sn
1	3.88	1.04	0.13	0.014	0.008	0.051	0.023	0.037	0.037	0.009
2	3.86	1.24	0.13	0.014	0.008	0.053	0.022	0.035	0.036	0.009
3	3.84	1.48	0.13	0.013	0.007	0.053	0.020	0.035	0.036	0.009
4	3.81	1.71	0.13	0.014	0.007	0.052	0.022	0.036	0.037	0.009
5	3.73	1.90	0.13	0.013	0.007	0.051	0.020	0.034	0.036	0.009
6	3.72	2.10	0.13	0.014	0.007	0.049	0.022	0.034	0.037	0.009
7	3.67	2.31	0.13	0.013	0.008	0.052	0.020	0.034	0.037	0.010
8	3.63	2.51	0.13	0.014	0.007	0.050	0.022	0.035	0.037	0.010
9	3.57	2.72	0.13	0.014	0.007	0.051	0.022	0.034	0.038	0.010
10	3.54	2.91	0.13	0.015	0.007	0.050	0.022	0.033	0.038	0.010
11	3.52	3.05	0.13	0.014	0.007	0.052	0.020	0.033	0.038	0.010
12	3.44	3.29	0.13	0.014	0.007	0.053	0.020	0.033	0.038	0.010
13	3.42	3.47	0.13	0.015	0.007	0.051	0.022	0.032	0.039	0.010
14	3.37	3.70	0.13	0.015	0.007	0.053	0.020	0.033	0.039	0.010
15	3.33	3.88	0.13	0.015	0.007	0.053	0.022	0.034	0.040	0.010
16	3.25	4.21	0.13	0.015	0.007	0.052	0.022	0.034	0.041	0.010
17	3.19	4.28	0.13	0.016	0.007	0.050	0.020	0.032	0.040	0.011
18	3.09	4.49	0.13	0.016	0.007	0.051	0.022	0.032	0.039	0.010
19**	3.06	4.75	0.13	0.016	0.007	0.052	0.020	0.033	0.040	0.011
20**	3.04	5.03	0.14	0.014	0.007	0.053	0.020	0.033	0.040	0.011
21**	2.95	5.45	0.14	0.015	0.007	0.053	<0.020	0.032	0.040	0.011
22**	2.85	5.64	0.14	0.017	0.007	0.048	0.023	0.035	0.040	0.011

Appendix A

Table AI. Characteristic temperatures, T_{LA} and $T_{e,min}$, from all cooling curves and recalescence Rec=($T_{e,max}$-$T_{e,min}$). All in Celsius. Two digits have been kept for recalescence as this is a relative value. Cups #.2 and #.3 were cubic (SQ) and cups #.4, #.5 and #.6 were cylindric (RD). ** indicates when double-coated cups were used.

Test	Cup Reference	T_{LA}	$T_{e,min}$	Rec
1	1.2	1170.3	1130.2	0.00
	1.3	1170.9	1131.6	0.00
	1.4	1163.7	1132.7	0.11
	1.5	1163.3	1132.3	0.28
	1.6	1165.8	1132.8	0.14
2	2.2	1161.5	1128.9	0.03
	2.3	1160.8	1128.9	0.00
	2.4	1160.0	1130.1	0.02
	2.5	1156.1	1128.0	0.00
	2.6	1162.1	1130.0	0.05
3	3.2	1160.1	1123.5	0.00
	3.3	1160.6	1124.0	0.00
	3.4	1157.9	1127.5	0.00
	3.5	1158.5	1126.9	0.02
	3.6	1160.7	1125.9	0.00
4	4.2	1158.5	1120.0	0.00
	4.3	1158.5	1121.2	0.00
	4.4	1156.9	1123.9	0.15
	4.5	1158.4	1123.2	0.03
	4.6	1153.7	1122.2	0.00
5	5.2	1155.8	1118.5	0.00
	5.4	1152.9	1118.9	0.00
	5.5	1153.5	1121.6	0.01
	5.6	1151.0	1120.6	0.04
6	6.2	1154.1	1116.7	0.00
	6.3	1154.8	1117.1	0.10
	6.4	1149.4	1115.2	0.00
	6.5	1149.9	1116.8	0.00
	6.6	1149.0	1115.3	0.00
7	7.2	1152.4	1112.1	0.00
	7.4	1150.2	1113.3	0.00
	7.5	1148.2	1112.1	0.00
	7.6	1151.9	1114.0	0.00

8	8.2	1152.5	1110.2	0.01
	8.3	1151.3	1110.3	0.00
	8.4	1149.4	1110.2	0.00
	8.5	1146.4	1109.2	0.00
	8.6	1148.5	1110.6	0.00
9	9.2	1150.6	1105.3	0.00
	9.3	1150.0	1107.3	0.00
	9.4	1149.3	1107.1	0.00
	9.5	1146.7	1105.9	0.00
	9.6	1148.5	1106.7	0.00
10	10.2	1150.0	1102.9	0.00
	10.4	1146.2	1102.5	0.00
	10.5	1145.7	1102.7	0.00
	10.6	1147.0	1104.2	0.00
11	11.2	1149.8	1100.7	0.00
	11.3	1150.6	1100.2	0.00
	11.4	1146.7	1099.8	0.00
	11.5	1144.9	1100.6	0.33
	11.6	1147.7	1100.1	0.00
12	12.2	1148.9	1095.7	0.00
	12.3	1149.8	1097.1	0.01
	12.4	1147.5	1096.6	0.03
	12.5	1147.9	1096.2	0.00
	12.6	1146.8	1097.3	0.00
13	13.2	1150.1	1093.2	0.00
	13.3	1151.1	1092.9	0.00
	13.4	1146.1	1094.0	0.00
	13.5	1148.1	1093.3	0.00
	13.6	1145.1	1093.0	0.14
14	14.2	1148.0	1089.6	0.00
	14.3	1148.5	1089.4	0.00
	14.4	1148.0	1090.9	0.53
	14.5	1147.9	1089.6	0.08
	14.6	1147.8	1089.8	0.08
15	15.2	1150.6	1085.6	0.00
	15.3	1149.1	1085.9	0.00
	15.4	1144.9	1087.7	0.49
	15.5	1147.5	1087.2	0.46
	15.6	1147.6	1087.5	0.66
16	16.2	1147.1	1081.9	0.00
	16.3	1145.2	1081.5	0.00
	16.4	1143.5	1082.2	0.03
	16.5	1143.4	1083.5	0.15
	16.6	1143.6	1083.4	0.03
17	17.2	1146.0	1078.0	0.00

	17.3	1145.8	1075.6	0.18
	17.4	1144.0	1079.3	0.40
	17.5	1143.9	1079.2	0.17
	17.6	1147.0	1079.9	0.61
18	18.2	1145.8	1074.9	7.20
	18.3	1146.0	1075.3	6.98
	18.4	1144.7	1077.0	1.25
	18.5	1146.5	1074.8	0.24
	18.6	1144.4	1076.0	1.79
19	19.2**	1152.8	1071.5	4.33
	19.3	1151.6	1072.7	5.60
	19.4**	1151.1	1071.5	1.78
	19.5**	1153.0	1071.3	1.35
	19.6	1147.8	1071.5	0.10
20	20.2**	1154.5	1065.9	0.00
	20.3	1150.6	1070.7	39.10
	20.4**	1153.3	1069.0	2.30
	20.5**	1150.7	1068.6	10.81
	20.6	1151.4	1076.3	65.80
21	21.2**	1153.7	1062.2	9.50
	21.3	1153.3	1067.8	33.30
	21.4**	1156.5	1064.2	14.20
	21.5**	1157.0	1065.1	8.86
	21.6	1153.8	1067.8	15.26
22	22.2**	1152.1	1061.1	7.73
	22.3	1146.8	1069.1	31.40
	22.4**	1146.1	1068.8	46.60
	22.5**	1152.6	1065.6	35.20
	22.6	1148.0	1067.7	37.80

Appendix B

The presence of SC iron silico-carbide was looked for with various means in alloys with high silicon contents. A Bruker D8 Advance diffractometer equipped with a Cu cathode was used in θ-2θ configuration. Records were carried out on various locations of samples 16.5 and 19.5 that all appeared similar. Figure B1 shows the record from the middle of sample 19.5 where ferrite (α_{Fe}) and cementite (Fe_3C) were easily identified, leaving one peak at 35.5° that can be associated without much doubt to Fe_8Si_2C in agreement with the record 00-026-0798 of the Inorganic Crystal Structure Database (ICSD). The height of this line indicates that the SC fraction was low, consistent with the small amount of this phase reported by Kante and Leineweber [2] for alloys with 3.0 and 4.2 wt.% Si.

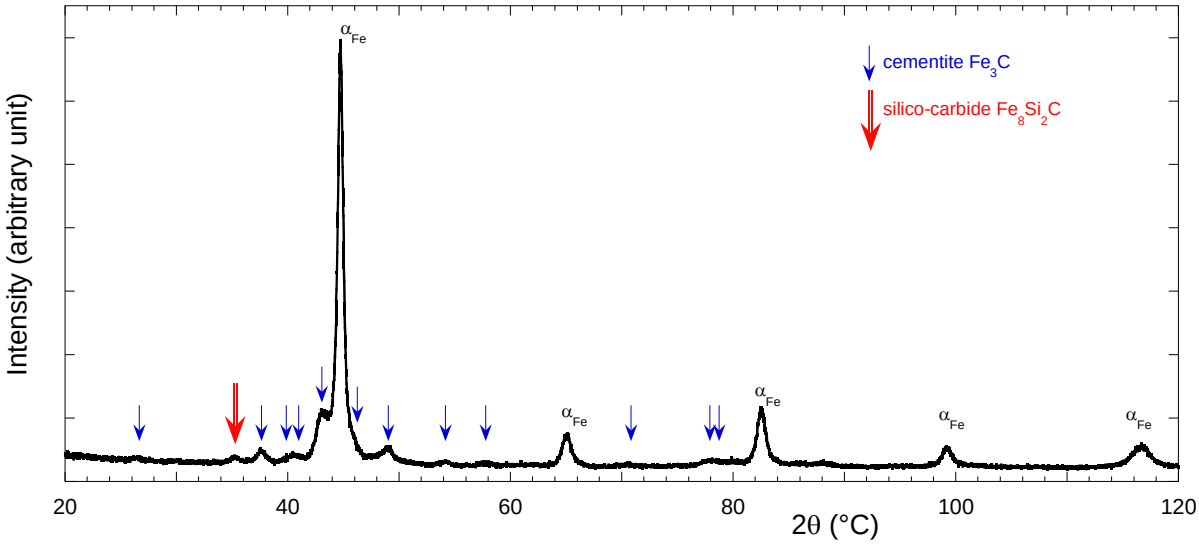

Figure B1. Experimental XRD pattern in the middle of sample 19.5 in which the main peaks are associated with ferrite (α_{Fe}). Only those peaks of cementite (Fe_3C) that are not superimposed to α_{Fe} peaks have been indicated with small arrows. One peak can be associated with Fe_8Si_2C that is indicated with the double arrow.

The existence of this silico-carbide was verified by metallographic observations on sample 19.5 under the scanning electron microscope (SEM). Figure B2 at low magnification shows interconnected graphite string cells in dark contrast in a variable gray contrast matrix. Close observation also reveals small white spots 20 µm in size that are undissolved Te particles. Figure B3 is an enlarged view of the matrix where the plate-like precipitates in light gray contrast are Fe_3C cementite and those in darker gray contrast are SC silico-carbide. This was verified by qualitative energy dispersive spectrometry (EDS) and is consistent with

observations reported by Kante and Leineweber. The remainder of the matrix consists of fine three-phase eutectic zones that were too fine to be properly resolved with the SEM used while the field electron gun SEM employed by Kante and Leineweber did.

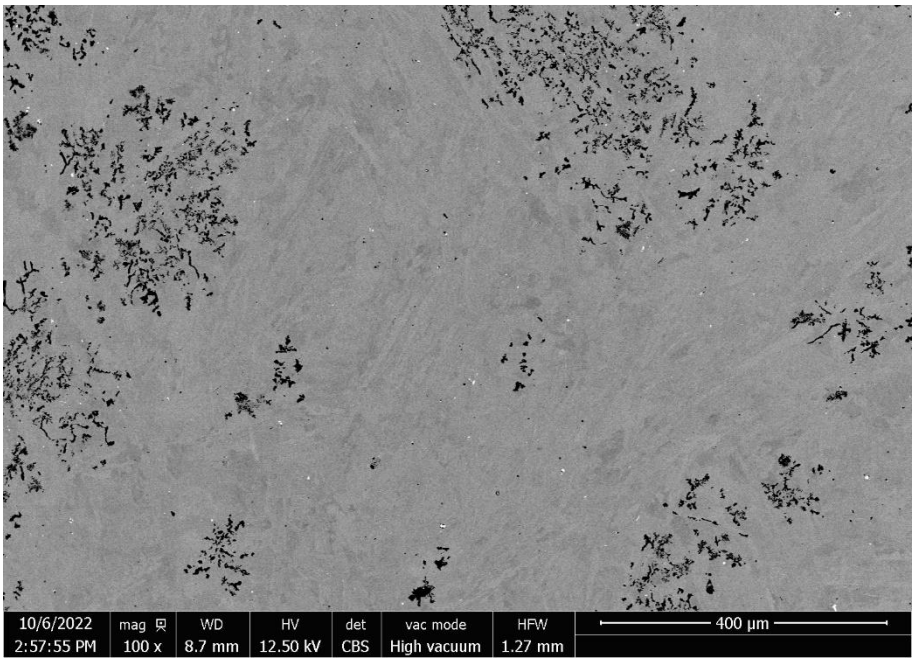

Figure B2. Low magnification SEM micrograph of the center of sample 19.5

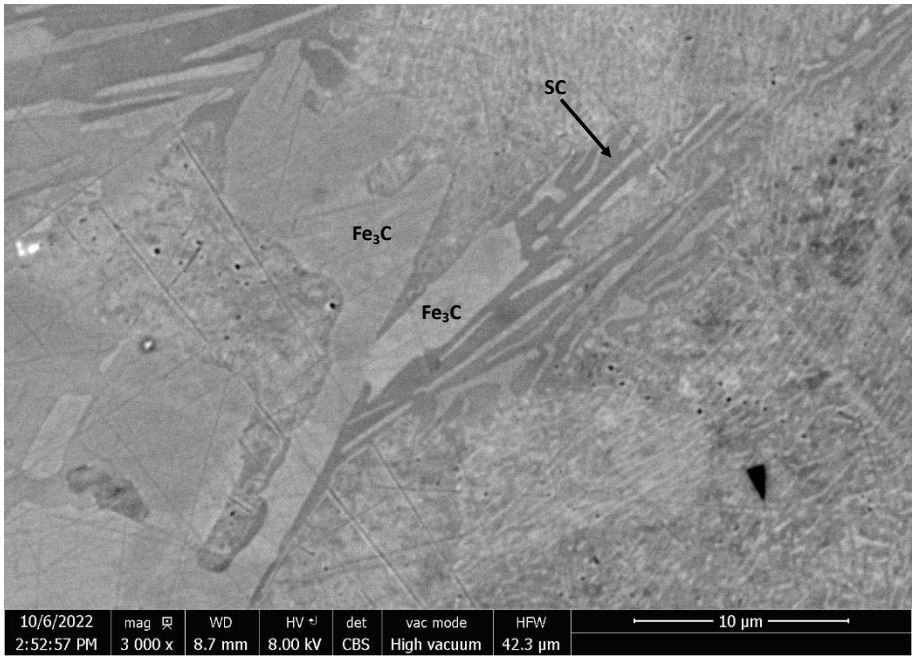

Figure B3. High magnification SEM micrograph of the matrix of sample 19.5.